Journal of Operations Intelligence, Volume 4, Issue 1 (2026) 42-64

Journal of Operations Intelligence

Journal homepage: www.jopi-journal.org
eISSN: 3009-4267

A Data-Driven Operations-Intelligence Framework for Lifecycle-Aware Maintenance Decision-Making Across Tramway Superstructure Variants

Vivien Révész-Jóvér[1], Szabolcs Fischer[1,*]

[1] Department of Transport Infrastructure and Water Resources Engineering, Széchenyi István University, Győr, Hungary

ARTICLE INFO

Article history:
Received 3 March 2026
Received in revised form 2 May 2026
Accepted 14 July 2026
Available online 17 July 2026

Keywords:
Tramway infrastructure; Predictive maintenance; Mixed-effects model; EN 13848 track twist; Bootstrap confidence interval; Lifecycle prediction; Elastically supported continuous rail bedding (ESCRB) rail; Concrete-slab track.

ABSTRACT

Urban-rail operators must convert routine track-geometry inspections into operational maintenance decisions across heterogeneous superstructures, yet age-based schedules and per-rail mean defects obscure the underlying deterioration mechanism. This paper develops an operations-intelligence framework that turns repeated geometric measurements into an explainable, data-driven ranking of sections by maintenance urgency. The framework is applied to 374,610 measurement points from 18 Budapest tramway sections, sampled 6 to 8 times over 2.3 years. Six analytical layers combine descriptive statistics; both-rail unified metrics including the EN 13848 track twist; an EN 13848-style Track Quality Index; hierarchical mixed-effects models; bootstrap ($B = 10{,}000$) and Theil–Sen confidence intervals; and AIC-based linear-versus-exponential model selection. Degradation proceeds mainly through twist generation – right- and left-rail slopes correlate strongly negatively ($r = -0.864$, $p < 0.0001$, $n = 18$). Concrete-slab gauge depends strongly on age ($R^2 = 0.72$, $n = 24$); mixed-effects models attribute 60.3% of gauge variance to between-section identity; the linear model is selected in 94% of fits; and a 3.0 mm threshold flags four sections for intervention within ten years. The pipeline feeds directly into operational decision-making and maintenance management systems and is transferable across sectors, relying on periodic condition monitoring.

1. Introduction

Maintenance of urban rail track assets sits at the intersection of three engineering disciplines: permanent way design, condition-based monitoring, and operational decision support. As city operators transition from fixed-interval inspection regimes toward genuine predictive-maintenance pipelines, they require quantitative tools that translate raw geometric measurements into actionable rankings of sections by maintenance urgency [1]. This deterioration is driven by identifiable physical mechanisms, notably the accumulation of differential settlement in zones of unsupported sleepers

[*] *Corresponding author.*
E-mail address: fischersz@sze.hu

https://doi.org/10.31181/jopi41202673

[2]. A growing body of data-driven and AI-based tools has been proposed to anticipate it [3, 4]. The challenge is non-trivial: rail networks operate mixed fleets of superstructure designs that age qualitatively differently, and the operational loads carried by individual sections vary by an order of magnitude across the network [5]. The wheel loads that individual sections actually carry can be quantified from axle loads using quasi-static wheel–rail load models [6]. Throughout this paper, the term *operations intelligence* denotes the systematic conversion of routine condition-monitoring data into explainable, decision-ready outputs — here, a transparent ranking of track sections by maintenance urgency — that an operator can act on without further interpretation; it is the analytical bridge between raw geometric measurement and the maintenance decision.

In the heavy-rail context, the European standard EN 13848-5 [7] has provided a stable answer to this question for more than two decades: standard deviations of longitudinal level, alignment, gauge, and cross-level are computed over fixed-length segments and compared against tiered thresholds (alert, alert action, intervention). In urban rail and especially in tramway operations, however, no comparable harmonized framework has gained traction. Two structural reasons account for the lacuna. First, the standard 200 m segment length adopted in EN 13848 often exceeds the length of a tramway test section. Second, the dominant superstructure designs in urban rail – concrete-slab tracks and continuously embedded resilient systems – behave physically very differently from the ballasted tracks for which the EN 13848 thresholds were calibrated [8]. These structural differences also have downstream consequences: track condition influences vehicle-side quantities such as running resistance and traction energy use [9], and condition assessment of discrete components such as crossings has been approached by combining statistical and mechanical reasoning [10].

The empirical record on tramway track-geometry deterioration has expanded substantially in the past five years. Multi-decade longitudinal datasets from Zagreb [5] and from selected Budapest lines [11–13]; probabilistic piecewise degradation models calibrated on mainline data provide the methodological backdrop [14]; the mechanical basis of such models — the rail treated as a beam on an elastic foundation — has been refined through new approximate analytical solutions [15]; and further degradation-modelling studies [16–18] have established that deterioration rates of urban tracks span a range nearly as wide as that observed on mainline networks, despite the lower axle loads. The original Budapest campaign [11, 12] focused on twenty-one sections representing seven superstructure variants and reported per-rail mean settlements, alignments, and gauge values across 6–8 measurement epochs spanning 2021–2023. As is appropriate for a first pass on a new dataset, the original analysis treated each rail of each section as an independent univariate time series, summarized by its absolute mean.

One remaining problem is the characterization of a single-track section in which the two rails are deteriorating in opposite directions. This problem is formulated by questions (i) to (iii). (i) The per-rail mean masks inter-rail asymmetry so strongly that so-called track twist defects can significantly affect the horizontal vehicle dynamics. (ii) Cross-sectional analyses of all sections of the six superstructure systems studied within this paper are problematic, since the sections of a single system were of different years of construction and even of different amounts of load. Thus, the partial identification of a system effect goes clearly beyond the indicators commonly used for condition assessment in practice [19]. (iii) The restriction of the use of the intervention data in an even stronger sense is due to the lack of a formal framework for the construction of confidence intervals for the per-section degradation slopes.

The authors introduce a statistical analysis framework that, within a single computational framework of six analysis layers ranging from simple summaries through modeling to prediction, answers all of the questions above for the first time. While each analysis layer is straightforward, the framework as a whole is novel and serves as the core of an emerging framework for urban rail asset management. The framework is here applied to the entire unique data set under study, comprising 18 sections of track from six different superstructure types, yielding some 374,610 individual measurements, to produce a single relational database. The resulting ranking of the sections by maintenance urgency accounts for the current geometric condition of the sections and predicts remaining life for two intervention thresholds.

The remainder of this paper is structured as follows. Section 2 surveys related work on tramway track geometry deterioration and on the EN 13848 framework. Section 3 specifies the data sources and instrumental properties. Section 4 develops the six-layer statistical framework. Section 5 presents the principal numerical results. Section 6 discusses practical implications and the limitations of the approach.

2. Related Work

2.1 Tramway track deterioration: longitudinal evidence

Ahac and Lakušić [5] established a multi-decade gauge-degradation model for tramway tracks on the Zagreb network, demonstrating that the cumulative gauge widening is well approximated by a power-law function of accumulated tonnage; piecewise-linear models of geometric evolution on mainline tracks provide a complementary methodological reference [14]. Their model – directly applicable to network-level planning – abstracts away from the question of which side of the track is responsible for the observed widening. Soleimanmeigouni *et al.,* [20] predicted geometry-defect evolution on a case-study line using probabilistic models that likewise aggregated over the two rails. The original Budapest studies [11–13] introduced the elastically supported continuous rail bedding (ESCRB I-III) [13] as an explicit category of analysis; related work has examined how superstructure maintenance affects the track geometry of regional lines [21] and the long-term behavior of resiliently padded concrete sleepers on reduced ballast beds [22]. Still, they retained the per-rail mean as the primary summary statistic. The present paper extends this line of work by lifting the per-rail-mean restriction and revisiting the same Budapest data under the joint inter-rail framework.

2.2 EN 13848 and the segment standard deviation

Soleimanmeigouni *et al.,* [1] surveyed thirty years of mainline track-geometry modeling and identified the segment standard deviation as the de facto industry-standard summary statistic, with the EN 13848-5 200 m segment length and the EN 13848-1 D1 wavelength band (3–25 m) as the dominant choices. The transfer of these conventions to urban tramway practice has been incremental. Farkas [23] reviewed inertial track-geometry measurement practice and segmenting conventions, and related work has extended geometry-based quality assessment toward automated defect detection [24, 25]. Berawi *et al.,* [26] argued for a 25 m segment as the most appropriate compromise between sample size and spatial resolution, consistent with later track-quality-index and segmentation studies [27–29]. The present paper adopts the 25 m segment convention.

2.3 Mixed-Effects Models in Railway Condition Monitoring

The use of hierarchical linear mixed-effects models for railway condition data is comparatively recent. Sysyn and co-workers [30, 31] applied random-intercept models to crossing-defect data. They recovered intraclass correlation coefficients of approximately 0.5 for vertical deflection, demonstrating that approximately half of the observed variance is attributable to persistent crossing-by-crossing differences; in a related vein, Andrade and Teixeira [32] modeled mainline track-geometry degradation with hierarchical Bayesian models. Sysyn *et al.,* [33] linked ballast interlocking and residual stress to load-dependent settlement behavior in heavy-haul tracks. To the best of the authors' knowledge, the present paper is the first application of mixed-effects variance partitioning to a multi-section tramway dataset.

2.4 Twist Generation and Asymmetric Settlement

The mechanism by which a symmetric ballast or slab initially settles preferentially under one rail has received considerable attention over the past five years. Sysyn *et al.,* [34] used track-side inertial monitoring and machine-learning analysis to demonstrate that the residual rail-base displacement after a fixed number of load cycles is asymmetric whenever the lateral force component at the wheel-rail interface is non-zero, even when the vertical component is symmetric. This residual-settlement behavior has been characterized at the ballast-box and grain scale [35, 36] and complemented by track-level methods for detecting localized ballast breakdown [37]. Kou *et al.,* [38] documented the closely related process at crossings, where crossing wear governs rolling-contact-fatigue damage of the frog rail, and localized crossing deterioration has been quantified from axle-box acceleration and train-hunting analyses [39, 40]; by analogy, the present paper attributes cant (twist) defect growth on tangent track sections to the same asymmetric residual-displacement mechanism. The present paper provides what appears to be the first quantitative confirmation of this mechanism across an entire tramway network.

2.5 Cognitive Mobility and the Operator Perspective

The cognitive-mobility framework [41–44] reframes urban-mobility quality assessment to integrate the cognitive and perceptual dimensions of movement experience. This perspective also connects to the broader mobility demand generated by ongoing agglomeration development [45] and to the broader sustainability agenda, including the decomposition of transport-related carbon dioxide emissions [46] and the optimization of multimodal freight routing [47]. For tramway operators, this reframing has three practical implications: ride-quality perception scales with the lateral and vertical acceleration content excited by twist and settlement defects in the 0.5–5 Hz range; rolling-stock dynamic response, and hence wear, scales with the time-integrated track-geometry quality, which onboard tram vehicle-dynamics measurements make directly observable [48]; and the visible cleanliness and audible smoothness of the line both feed back into modal-choice behavior, an outcome increasingly emphasized in sustainable-mobility transport policy [49]. A quantitative ranking of superstructure variants by geometric deterioration rate is therefore a foundational input to subsequent cognitive-mobility-aware decisions.

3. Data

3.1 Test-Section Selection and Measurement Campaign

Eighteen test sections in operational service on the Budapest tramway network were measured repeatedly between June 2021 and October 2023 (Table 1).

Table 1
Eighteen test sections grouped by superstructure variant, with installation year, annual load, and number of measurement runs

Section	Variant	Installed	Load [MGT/y]	# runs	Rail/embedment/sleeper
ZK-1	Ballasted	1985	1.97	8	54E1 Vignol rail / crushed-stone ballast / RC sleeper
ZK-2	Ballasted	1987	1.19	8	Vg48 Vignol rail / crushed-stone ballast / RC sleeper
ZK-3	Ballasted	2002	3.92	8	49E1/MA48 Vignol rail / crushed-stone ballast / RC sleeper

Table 1
Continued

Section	Variant	Installed	Load [MGT/y]	# runs	Rail/embedment/sleeper
ZK-4	Ballasted	2018	5.73	8	MA48 Vignol rail / crushed-stone ballast / RC sleeper
BL-1	Concrete-slab	1986	4.15	8	54E1 rail / direct fastening / cast RC slab
BL-2	Concrete-slab	2001	6.90	8	MA48 rail / ICOSIT underpour/cast RC slab
BL-3	Concrete-slab	2010	4.62	8	49E1 rail / ICOSIT underpour/cast RC slab
RF.I-1	ESCRB I	2008	4.12	6	59R2 grooved rail/rubber profile / Gantry clip
RF.I-2	ESCRB I	2003	3.77	6	59R2 grooved rail/rubber profile / Gantry clip
RF.I-3	ESCRB I	2014	6.98	6	59R2 grooved rail/rubber profile / Gantry clip
RF.II-1	ESCRB II	2011	4.72	6	59R2 grooved rail / CDM profiles / RC slab
RF.II-2	ESCRB II	2014	5.74	6	59R2 grooved rail / CDM profiles / RC longitudinal beam
RF.II-3	ESCRB II	2016	9.18	6	59R2 grooved rail / CDM profiles / RC slab
RF.II-4	ESCRB II	2014	4.30	6	59R2 grooved rail / CDM profiles / RC slab
RF.III-1	ESCRB III	2001	6.90	6	51R1 grooved rail / Edilon Corkelast / bridge RC slab
RF.III-2	ESCRB III	2009	4.12	6	53R1 grooved rail / Edilon Corkelast / RC slab
RF.III-3	ESCRB III	2014	6.97	6	51R1 grooved rail / Edilon Corkelast / bridge RC slab
RF.III-4	ESCRB III	2018	12.84	6	59R2 grooved rail / SIKA embedment / RC slab

The sections collectively represent six superstructure systems: four ballasted (ZK) sections, three concrete-slab (BL) sections, three ESCRB I sections, four ESCRB II sections, and four ESCRB III sections. Each open (non-embedded) section was measured eight times across the campaign; each embedded section was measured six times. Sections were selected to span installation years from 1985 to 2018 and annual loads from 1.19 to 12.84 million equivalent gross tons (MGT) per year. Geometric measurements within switches, road crossings, or sharp curves were excluded by construction. A complete listing of section attributes is given in Table 1.

Throughout the observation period, the eighteen sections remained in normal revenue service, and the campaign captured their as-operated geometric condition rather than any response to scheduled renewal. To the authors' knowledge, no major restorative maintenance — such as tamping, gauge correction, or rail replacement — was performed on the investigated sections between the first and last measurement epochs, and every epoch was therefore retained in the analysis. This is corroborated by the trend results in Section 5, which show that no section exhibits a statistically significant negative (improving) settlement slope; a restorative intervention would instead appear as an abrupt improvement in geometric quality. Where the framework is applied to a section that does undergo such an intervention within the monitoring window, the affected series should be segmented at the intervention date and the degradation slope re-estimated on the post-intervention epochs alone, since pooling measurements across the discontinuity would bias the estimated slope toward zero and overstate the projected remaining life.

3.2 Instrument and Sampling Protocol

All measurements were performed with the TrackScan ME 4.01 hand-held continuous track-geometry instrument, manufactured by Metalelektro Méréstechnika Ltd. (Budapest, Hungary). The instrument records five geometric quantities simultaneously at 0.25 m increments along the track:

the track gauge (manufacturer specification ±0.01 mm), the lateral alignment of each rail (asymmetric 1.510 m three-point chord, ±0.025 mm), the longitudinal level (settlement) of each rail (asymmetric three-point chord, ±0.025 mm), and the radius of curvature [50]. Complementary condition information in potentially critical track zones can be obtained from vibration-based response measurements [51]. Measurements were conducted during nighttime traffic-free windows between 01:00 and 04:00 local time. The eighteen sections together comprise 374,610 measurement points across the campaign.

3.3 Data Pre-Processing and Quality Control

Raw instrument output was ingested into a structured relational database (Python 3.12, pandas 2.x) after applying three quality-control filters. First, any measurement record with anomalous chainage increments (deviations from 0.25 m exceeding 0.05 m) was inspected manually and either corrected (when the cause was an instrument repositioning event) or rejected. Second, the two rail sides were aligned to a common chainage axis by interpolation when their native sampling grids differed, affecting fewer than 0.1% of all paired observations. A third aspect was that three sections (BL-2 in late 2022 and early 2023) used an internal index for the rail-alignment parameters, which differed from the chainage. This was noted, cross-referenced with the chainage column and then corrected as part of the pre-processing. The resulting data consist of 374,610 tuples of (section, date, chainage, parameter) and are in 'long' format.

4. Statistical Framework

The analysis framework is structured into 6 layers, depicted in Figure 1 and explained in more detail below.

Thus, the layers of analysis range from data-near descriptive analysis via empirical models and hypothesis testing to more or less extrapolative prediction. Beyond the six-layer schematic, Figure 1 doubles as a graphical abstract of the study's four principal empirical findings, shown in Panels A–D; each panel summarizes a result developed in full later in the paper and is presented here only to orient the reader. Panel A reports the settlement degradation rate across the superstructure variants (the per-section and per-variant rates analyzed in Sections 5.1 and 5.6). Panel B is the scatter of right- against left-rail settlement slopes, whose strong negative correlation ($r = -0.864$, $p < 0.0001$; reported in Section 5.8) is the signature of twist generation and the empirical motivation for the both-rail unified metrics introduced in Section 4.2. Panel C shows the age dependence of track-gauge widening on the concrete-slab (BL) sections ($R^2 = 0.72$; Section 5.8). Panel D shows the pooled time evolution of settlement per system, which serves as the raw material for the trend estimation in Section 4.4 and the lifetime projection in Section 5.4. The panels are therefore outputs that summarize the analysis rather than inputs to it, and each is cross-referenced at the point where it is derived.

4.1 Layer 1 – Per-Rail Descriptive Statistics

For each (section, measurement date, geometric parameter) tuple, the following per-rail summary statistics are computed: arithmetic mean, absolute mean defined as the average of $|x|$ over all chainage points, sample standard deviation, median, the 25th and 75th percentiles, the 95th and 99th percentiles of $|x|$, the root-mean-square *RMS* defined by Eq. (1), the third standardized moment (skewness), and the fourth standardized moment (excess kurtosis). These statistics constitute the data-near layer of the framework, preserving as much distributional information as can be summarized in scalar form.

$$\mathrm{RMS} = \sqrt{\langle x^2 \rangle} \tag{1}$$

where RMS is the root-mean-square of the per-rail geometric parameter, x denotes the parameter value at an individual chainage point, and $\langle\cdot\rangle$ denotes the arithmetic mean (averaging operator) taken over all chainage points of the section.

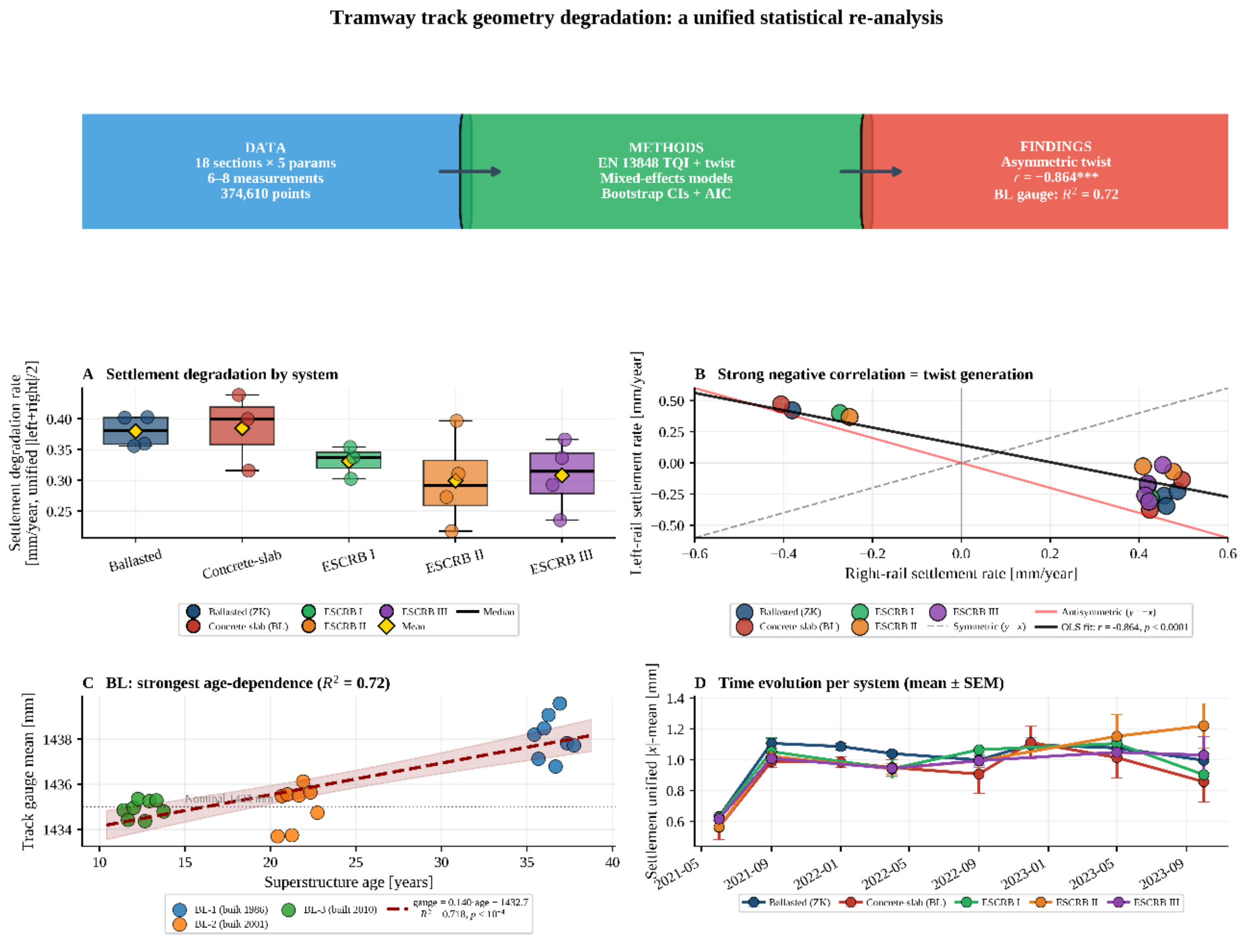

Fig. 1. Graphical abstract of the six-layer framework with key empirical findings. Panel A: settlement degradation rate across the five superstructure variants. Panel B: scatter of right- vs. left-rail settlement slopes (strong negative correlation indicates twist generation). Panel C: track-gauge widening with section age on concrete-slab (BL) sections. Panel D: pooled time evolution of settlement per system.

4.2 Layer 2 – Both-Rail Unified Metrics

Three unified metrics that combine the two rails of a section are defined to address the asymmetry identified in Section 1. For settlement (the same definitions apply to alignment), the both-rail absolute mean $AM_{unified}(s)$ is defined point-wise as in Eq. (2), the both-rail root-mean-square $RMS_{unified}(s)$ as in Eq. (3), and the EN 13848 track twist $TW(s)$ as in Eq. (4):

$$AM_{unified}(s) = \frac{|r(s)|+|l(s)|}{2} \tag{2}$$

$$RMS_{unified}(s) = \sqrt{\frac{r^2(s)+l^2(s)}{2}} \tag{3}$$

$$TW(s) = |r(s) - l(s)| \tag{4}$$

where $AM_{unified}(s)$, $RMS_{unified}(s)$ and $TW(s)$ are, respectively, the both-rail unified absolute mean, the both-rail unified root-mean-square and the EN 13848 track twist evaluated point-wise at chainage s; $r(s)$ and $l(s)$ denote the right- and left-rail settlement (or alignment) values at chainage s; and $|\cdot|$ denotes the absolute-value operator.

Each quantity is summarized over the section by its arithmetic mean, by its 95th percentile, and by its maximum. The track twist, as defined here, is the urban-rail equivalent of the EN 13848-1 "track twist" parameter, which is computed in heavy-rail practice over a 3 m base length using cross-level (cant) measurements. For the unloaded measurement frame used here, the point-wise difference of the two rail settlements provides a direct analog.

4.3 Layer 3 – EN 13848-Style Track Quality Index

Each section is partitioned into non-overlapping 25 m segments (corresponding to 100 chainage points at the native sampling). For each segment, the sample standard deviation of the parameter value is computed. The Track Quality Index for the section is then defined as the arithmetic mean across all valid segments of the segment-wise standard deviation, as given by Eq. (5):

$$TQI = \mathrm{mean}_{segments}\sigma_{segment} \tag{5}$$

where TQI is the Track Quality Index of the section, $\sigma_{segment}$ is the sample standard deviation of the geometric parameter within a single 25 m segment, and $\mathrm{mean}_{segments}$ denotes the arithmetic mean taken over all valid 25 m segments of the section.

This is a direct adaptation of the EN 13848 segment-statistic approach to the smaller sections typical of tramway test campaigns. The 25 m choice approximately preserves the D1 wavelength band (3–25 m), which dominates the dynamic response of light-rail vehicles.

4.4 Layer 4 – Trend Estimation with Robust Confidence Intervals

For each (section, summary metric) pair, the temporal evolution of the summary across the 6 to 8 measurement epochs is modeled by simple linear regression of the summary on time (measured in years from the first measurement of that section). The Ordinary Least Squares (OLS) slope provides the central estimate of the degradation rate. A nonparametric paired bootstrap with $B = 10{,}000$ resamples is used to construct the 95% confidence interval on the slope; the Theil–Sen median-slope estimator is computed in parallel as a robustness check against influential observations. The statistical significance of an individual section's slope is assessed using two independent criteria: the OLS p-value at the 0.05 level and whether the 95% bootstrap confidence interval excludes zero. Autocorrelation of regression residuals is tested using the Durbin-Watson statistic.

4.5 Layer 5 – Hierarchical Variance Decomposition

A linear mixed-effects model is fitted to each summary metric across the full set of *(section × measurement-date)* observations. The fixed-effects structure includes the time variable, the superstructure variant as a categorical predictor, and their interaction. The random-effects structure includes a random intercept for section identity. From the estimated random-effect variance $\sigma^2_{section}$ and residual variance $\sigma^2_{residual}$, the intraclass correlation coefficient ICC is computed as in Eq. (6):

$$ICC = \frac{\sigma^2_{section}}{\sigma^2_{section} + \sigma^2_{residual}} \tag{6}$$

where *ICC* is the intraclass correlation coefficient, $\sigma^2_{section}$ is the random-effect (between-section) variance, and $\sigma^2_{residual}$ is the residual (within-section) variance, both estimated by the linear mixed-effects model.

The *ICC* has a direct interpretation: it represents the fraction of the total variance, after controlling for the fixed-effects structure, attributable to persistent between-section differences (e.g., installation tolerances, age, structural detail, accumulated load history). All models are fitted by restricted maximum likelihood using the statsmodels MixedLM implementation. An analysis of covariance (ANCOVA) with section-level slopes as the dependent variable, superstructure variant as a categorical predictor, and section age and annual load as covariates is also fitted to test whether the variant effect persists after adjusting for the two confounders.

4.6 Layer 6 – Model Selection and Lifetime Extrapolation

For each (section, summary metric) pair, two candidate temporal models are fitted to the summary metric as a function of time: a linear temporal model, given by Eq. (7), and an exponential temporal model, given by Eq. (8):

$$y(t) = a \cdot t + b \tag{7}$$

$$y(t) = c \cdot \exp(k \cdot t) \tag{8}$$

where $y(t)$ is the value of the summary metric at time t (measured in years from the first measurement of the section), a and b are the slope and intercept of the linear model, c and k are the scale and growth-rate parameters of the exponential model, and exp denotes the exponential function.

Their Akaike information criterion values are compared. The model with lower AIC (Akaike Information Criterion) is selected; a tabulation of the selection outcome across all (section, metric) pairs provides an evidence-based answer to the long-debated question of whether tramway track geometry deteriorates linearly or exponentially on the multi-year scale within a single maintenance cycle. A tentative intervention threshold ϑ is then specified (for the both-rail unified settlement absolute mean, ϑ = 3.0 mm, corresponding to approximately twice the median end-of-campaign value across the dataset). The choice of 3.0 mm is deliberately relative rather than absolute: fixing the trigger at roughly twice the dataset-wide median end-of-campaign value means that a section reaching it has departed clearly from the population of normally fluctuating in-service values and can be treated as a genuine outlier that warrants attention, instead of being flagged against an arbitrary fixed limit. Expressing the threshold in the both-rail unified settlement — the quantity whose inter-rail twist component drives the lateral and vertical vehicle dynamics discussed in Section 2.5 — keeps the trigger tied to the ride-quality and safety consequences that ultimately justify intervention. The value is explicitly tentative and is intended to be recalibrated against each operator's own acceptance limits and historical maintenance records; because the remaining-life estimate of Eq. (9) contains θ only in its numerator, the framework recomputes both the projected horizons and the resulting section ranking transparently for any operator-selected threshold. The remaining lifetime for each section is computed by linear extrapolation of the section-level slope, as given by Eq. (9):

$$T_{rem} = \frac{\vartheta - y_{cur}}{a_{us}} \tag{9}$$

where T_{rem} is the projected remaining lifetime of the section, ϑ is the intervention threshold, y_{cur} is the most recent observed value of the unified settlement, and a_{us} is the section-level degradation slope of both-rail unified settlement.

This is recognized as a first-order projection that ignores any non-linear acceleration toward the end of life; it is included in the framework as a practical input to maintenance planning rather than as a definitive lifetime statement.

5. Results

5.1 Heatmap of Per-Section Per-Metric Degradation Rates

Figure 2 is a compact representation of all 18 test sections of the degradation landscape. Each row in the resulting heatmap represents the seven metrics for a given group of test sections: the gauge mean, the two metrics for right- and left-rail alignment, and the two metrics for right- and left-rail settlement. For each group of metrics, the metrics for both rails are averaged, and for the alignment metrics, the averaged values for both rails are also included. The columns of the heatmap represent the test sections, sorted by superstructure, and the cell values are the OLS-slope values in mm/year. Red-colored values indicate positive values; thus, the section is degrading. Blue-colored values indicate negative values, either indicating that the section is improving or that it is even subject to reverse degradation, even though the values are very noisy. Three main statements can be made from this figure. First, the gauge-mean row exhibits strong red shading across the ESCRB II group (RF.II-1 through RF.II-4) and considerably weaker shading elsewhere, indicating that the gauge widens fastest on this ESCRB system. Second, the settlement rows for the right rail are predominantly red across nearly all sections, whereas the left-rail rows alternate; this is the visual signature of the asymmetric degradation pattern analyzed in detail below. Third, the variability of the alignment rows is substantially smaller than that of the settlement rows, consistent with the smaller dynamic range of alignment defects in modern urban tracks.

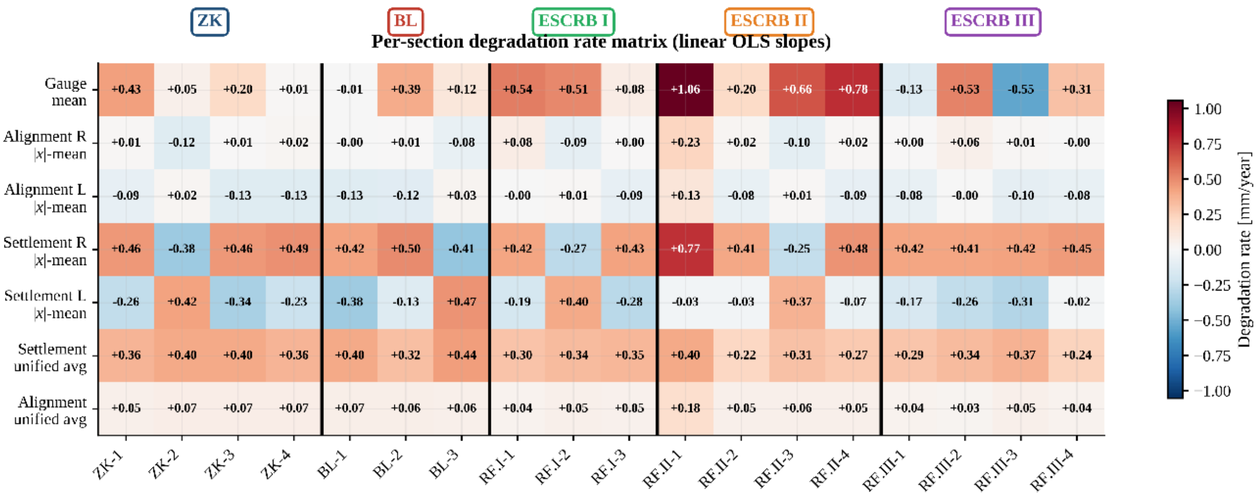

Fig. 2. Heatmap of degradation rates [mm/year] across all eighteen sections (columns) and seven summary metrics (rows). Color encodes the OLS regression slope; vertical black lines separate the superstructure variants. Numerical values are the slope estimates.

5.2 Distributional View of Settlement and Twist

Figure 3 transitions from the per-section rate view to the distributional view, presenting the cross-sectional distribution of two key indicators across all (section, measurement date) observations within each superstructure variant. Panel A shows the distribution of the absolute mean of the both-rail unified settlement. The ballasted ZK system has the highest median (≈1.0 mm) and the widest interquartile range, consistent with its lower vertical restraint. The four embedded systems (BL and the three ESCRB variants) have similar medians clustered around 0.85–0.95 mm and tighter interquartile ranges. Panel B shows the distribution of the EN 13848 track twist absolute mean. Here, too, the ZK system stands out – both medially (≈1.4 mm) and in the upper tail of the distribution – while the four embedded systems lie tightly clustered around a twist value of 1.2–1.3 mm. This visualization shows that differences among embedded variants are small on average, whereas the ballasted system is consistently the most defect-prone.

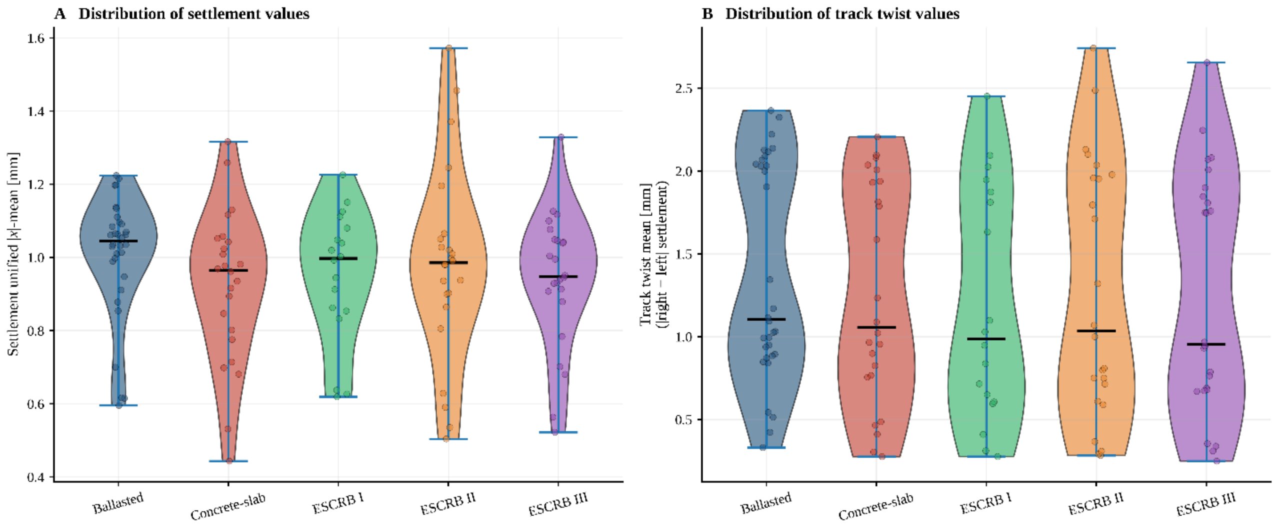

Fig. 3. Distribution of two unified geometric indicators across all (section, measurement date) observations grouped by superstructure variant. Panel A: both-rail unified settlement absolute mean. Panel B: EN 13848 track twist absolute mean (|right − left| settlement). Violin widths show kernel density estimates; thick horizontal lines indicate medians; dots indicate individual observations.

5.3 Bootstrap Forest Plot of Settlement Degradation Rates

Figure 4 presents the central per-section degradation result in the standard forest-plot format used in meta-analyses. For each of the eighteen sections, the bootstrap 95% confidence interval for both-rail unified settlement degradation slope is shown as a horizontal line, with the bootstrap mean as a filled marker and a red asterisk indicating intervals that exclude zero. Fourteen of the eighteen sections have a settlement slope whose 95% bootstrap CI (confidence interval) is strictly positive, a fraction (78%) that is internally consistent with the OLS-based significance counting reported in Section 5.4 below. The remaining four sections (BL-1, BL-2 (narrow CI), RF.I-2, ZK-2) have bootstrap intervals that include zero – either because the temporal trend is genuinely small or because the noise level is unusually high relative to the slope. Crucially, no section has a bootstrap CI that lies strictly in negative territory, ruling out any *genuine* improvement in settlement-related geometric quality across the campaign.

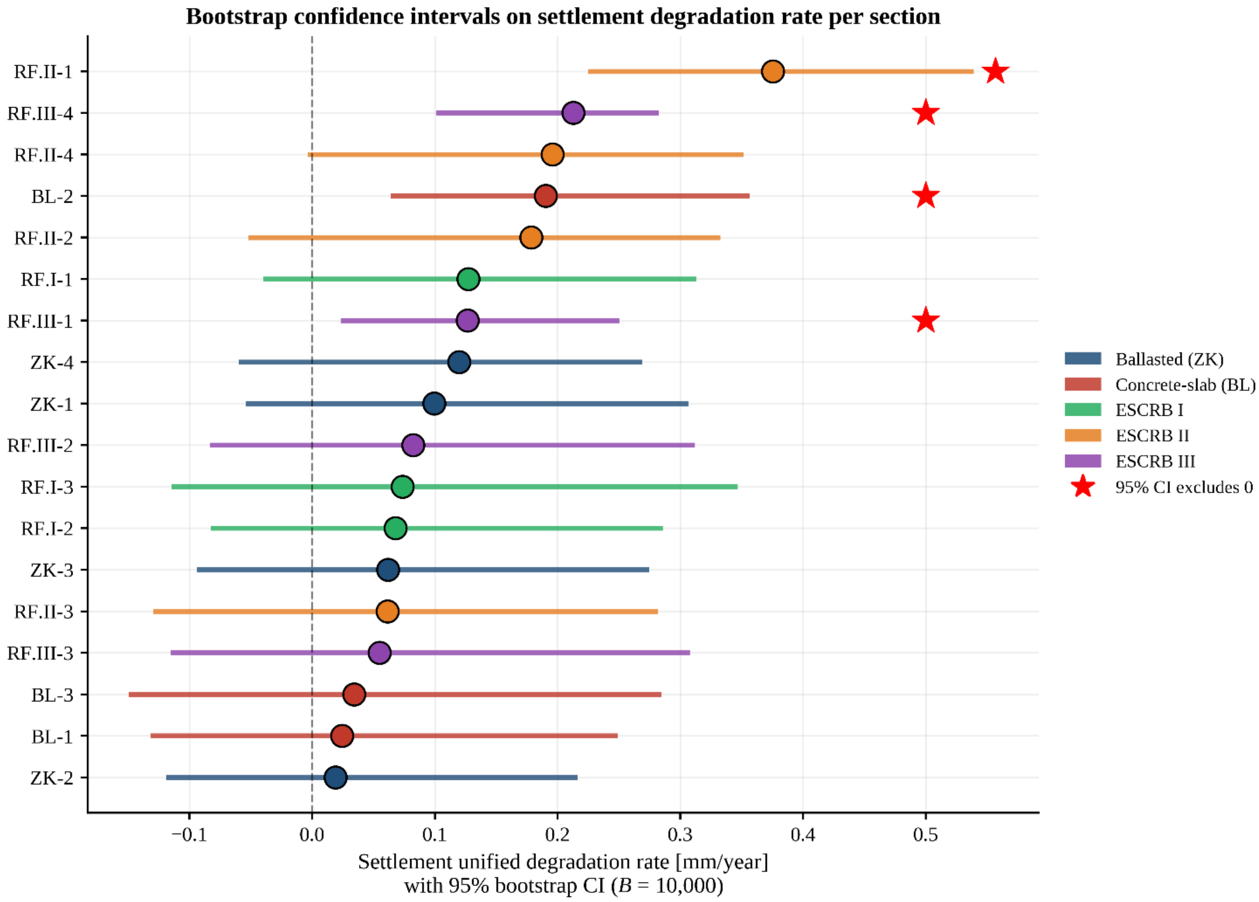

Fig. 4. Forest plot of section-level both-rail unified settlement degradation rates, sorted by the bootstrap mean. Horizontal lines: 95% bootstrap CI (B = 10,000); filled markers: bootstrap mean. Sections whose CI excludes zero are marked with a red asterisk (★).

5.4 Lifetime Projection and Maintenance Prioritization

Figure 5 combines the bootstrap-validated slopes with the most recent observed settlement value to project the time remaining until the unified settlement reaches the tentative 3.0 mm intervention threshold. Panel A displays the remaining-lifetime estimates, sorted in ascending order; sections with projected interventions within 10 years are highlighted in dark red. Four sections (RF.II-1, RF.III-4, RF.II-2, RF.II-4) project to require intervention within ten years; two more (BL-2, ZK-4) within fifteen years; and the remaining twelve sections within horizons of 20 years or longer. The four shortest-horizon sections share two features: they are all relatively recent installations (2011–2018) and carry high annual loads (4.30–12.84 MGT/year). Panel B presents the same information as a maintenance priority quadrant, with the current settlement state on the abscissa and the degradation rate on the ordinate. The upper-right quadrant (high current state, fast degradation, designated Priority 1) is empty in this dataset, but the upper-left quadrant (lower current state, fast degradation, Priority 2) contains all four of the short-horizon sections. The lower-right quadrant (Priority 3, high current state but slow degradation) contains a single section (BL-2), which is monitored but not currently scheduled for intervention. The lower-left quadrant (stable) accounts for the majority of sections.

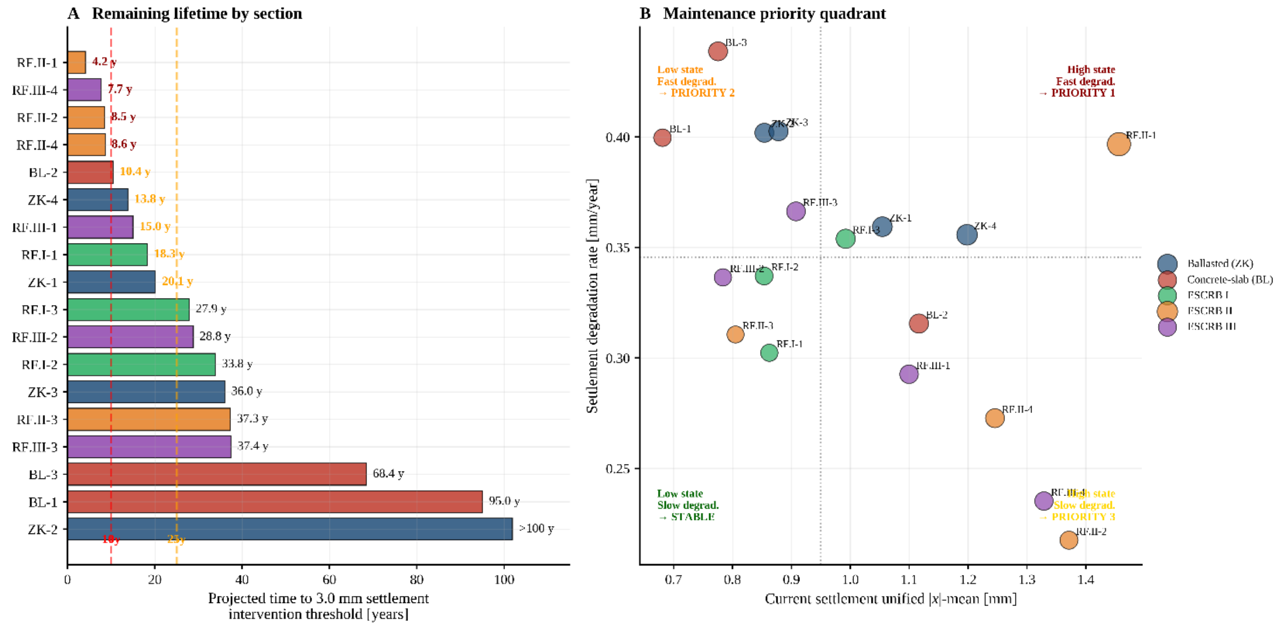

Fig. 5. Maintenance prioritization output. Panel A: remaining lifetime until the 3.0 mm unified settlement threshold, sorted ascending. Sections crossing the 10- and 25-year horizons are highlighted in dark red and orange, respectively. Panel B: priority quadrant with current state on the *x*-axis and degradation rate on the *y*-axis. Marker size encodes a combined urgency score. Quadrants are labeled by priority level.

5.5 Spatial-Temporal Evolution Along Selected Sections

Figure 6 zooms into three representative sections to display the spatial-temporal evolution of the right-rail settlement along the chainage axis.

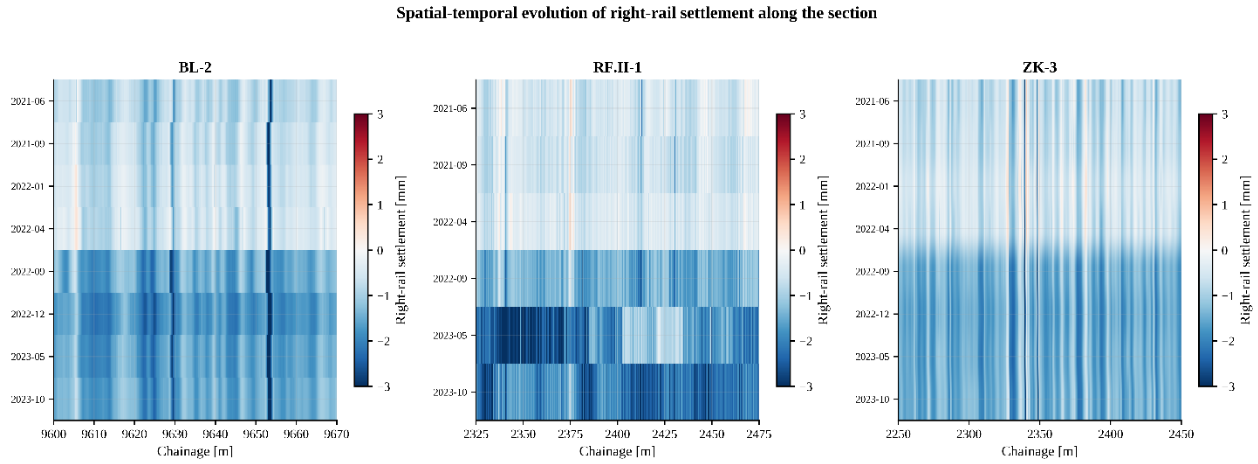

Fig. 6. Right-rail settlement evolution along chainage for three representative sections. Each row of each subpanel corresponds to a measurement epoch; colors encode the settlement value at each 0.25 m chainage point on a diverging red-to-blue scale.

Each row in each subpanel corresponds to a measurement epoch and is color-mapped using the same diverging scale (−3 to +3 mm). The BL-2 section (a 1986-installed concrete slab) shows a predominantly stable settlement pattern, with localized defects that do not migrate substantially between epochs. The RF.II-1 section (a 2011 ESCRB II installation) shows a clear progressive deepening of a localized defect near chainage 5400 m, visible as a deepening of the dark blue color in successive measurements. The ZK-3 section (a 2002 ballasted track on a high-load line) shows a complex pattern of localized defects that intensify with measurement date. Spatial-temporal displays of this kind are directly usable by maintenance engineers to identify defect-generating physical features such as inadequately drained substructure, sub-ballast voids, or substructure deformation.

5.6 Multi-Metric Superstructure Ranking

Figure 7 presents a radar (spider) comparison of the five superstructure variants on five normalized indicators: the classical right-rail settlement absolute mean, the both-rail unified absolute mean, the EN 13848 track twist, the EN 13848-style segment-SD-based TQI, and the settlement degradation rate. Each indicator is rescaled to the unit interval across the five systems so that 0 denotes the best system on that indicator and 1 the worst. No single superstructure variant dominates across all five indicators: ESCRB III is best on the classical right-rail mean; the *TQI*, the ballasted ZK system, is worst on twist and the unified mean; and ESCRB II is worst on the degradation rate. The visualization emphasizes that choices among the embedded variants should be made on grounds other than geometric quality (e.g., life-cycle cost, noise emission, retrofit complexity), since their geometric performance is essentially indistinguishable on the present indicators.

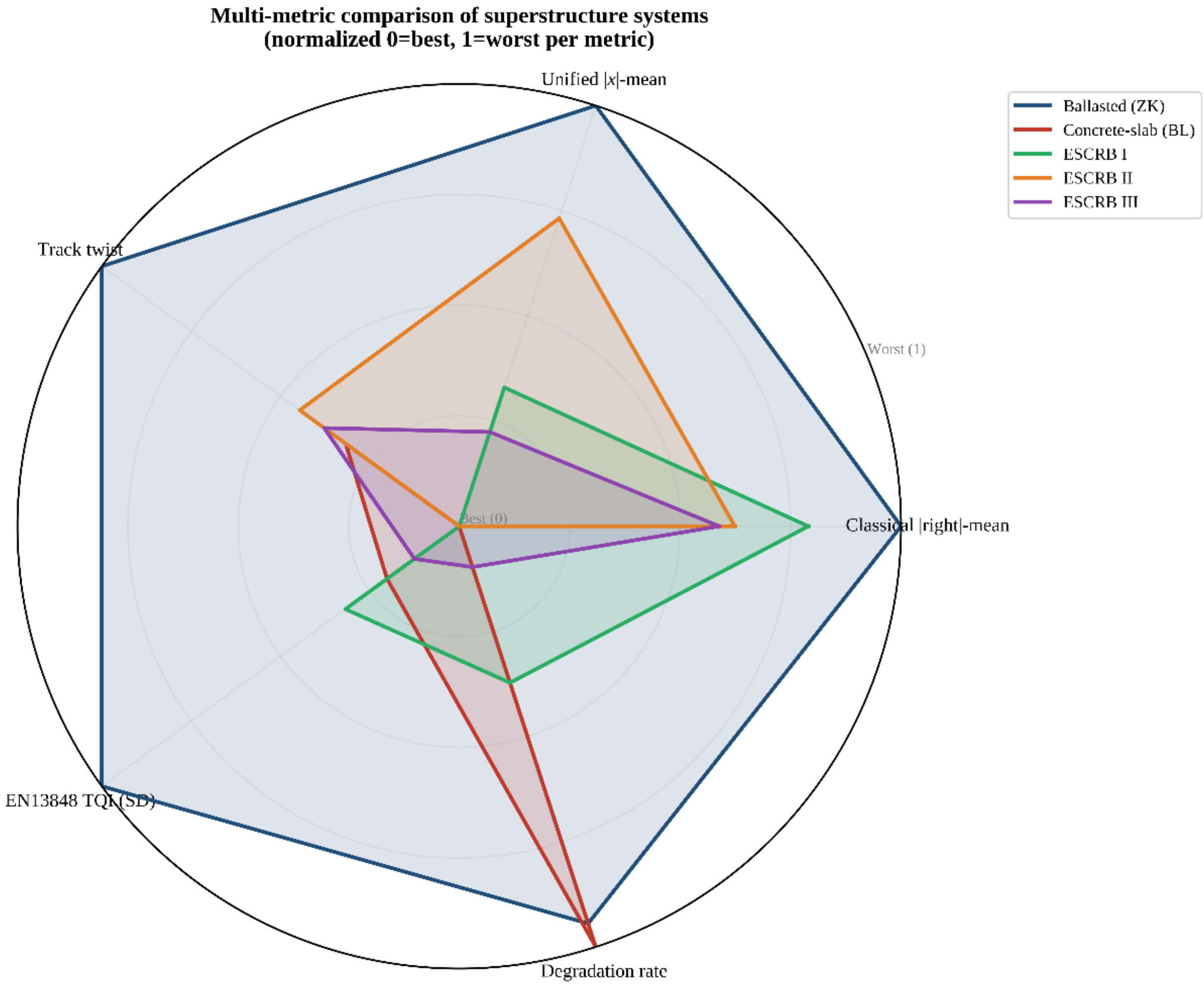

Fig. 7. Multi-indicator radar comparison of the five superstructure variants on five normalized geometric-quality indicators. Each indicator is rescaled to [0, 1] across the five systems (0 = best system, 1 = worst).

5.7 Variance Partitioning by Mixed-Effects Modeling

Figure 8 presents the variance-partitioning output of the hierarchical linear mixed-effects models fitted to four key summary metrics. Panel A shows the intraclass correlation coefficient (*ICC*) for each metric: for track gauge mean, the *ICC* is 0.672, indicating that two-thirds of the total variance, after controlling for time- and variant-fixed effects, is attributable to persistent between-section differences. For alignment, the unified *ICC* drops to 0.169; for the settlement and twist metrics, the random-intercept variance is effectively zero after the fixed-effects adjustment, indicating that the variant and time main effects fully account for the systematic variance. Panel B visualizes the per-section random-effect estimates for the gauge model, showing each section's deviation from the global mean gauge after controlling for variant and time. Eight sections (most prominently BL-1, BL-2, and BL-3) carry persistent positive random-effect estimates, while ten sections (most prominently the high-load ESCRB sections) carry persistent negative random effects. The magnitude of these random effects (roughly ±3 mm) is comparable to the within-section temporal trend, indicating that identifying an individual section's installation epoch is more important than observing its temporal trend for understanding its current gauge value.

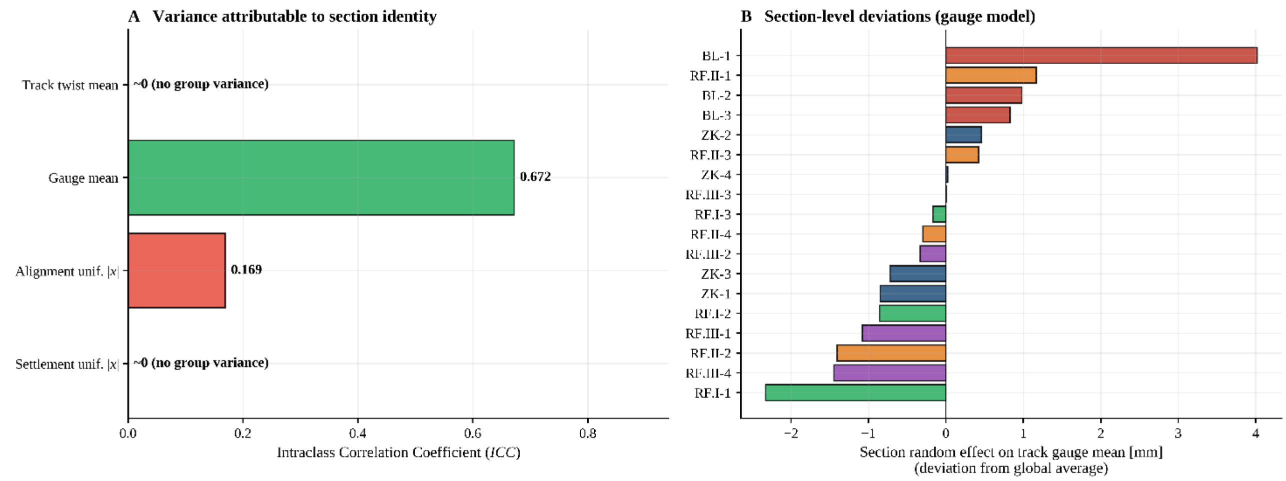

Fig. 8. Mixed-effects model output. Panel A: intraclass correlation coefficient (*ICC*) for four key summary metrics, indicating the fraction of total variance attributable to section identity. Panel B: per-section random-intercept estimates from the gauge model, sorted by magnitude.

5.8 Summary of Inferential Test Outcomes

The principal inferential test outcomes from the full statistical framework are summarized as follows. (i) The Pearson correlation between the right- and left-rail settlement slopes across the eighteen sections is $r = -0.864$ ($p < 0.0001$, $n = 18$), constituting strong evidence of antisymmetric settlement and of twist generation as the principal degradation mode. (ii) Restricted to the three concrete-slab BL sections, the cross-sectional regression of gauge mean on superstructure age yields slope = 0.140 mm/year, intercept = 1432.7 mm, $R^2 = 0.718$, $p < 0.0001$, $n = 24$, representing by far the strongest age-parameter relationship in the dataset. (iii) The Kruskal-Wallis test for differences in settlement degradation rate across the five superstructure variants yields $H = 7.41$ ($p = 0.116$, $n = 18$), indicating that the variant effect on settlement is marginal in the unadjusted comparison; the analogous test on alignment degradation rate yields $H = 10.23$ ($p = 0.037$, $n = 18$), reaching the conventional significance level. (iv) The linear-versus-exponential model comparison (54 section-metric pairs across three unified metrics) selects the linear model in 94.4% of cases by AIC, with a mean $\Delta AIC = +0.56$ favoring linearity. (v) The Brown–Forsythe test for homogeneity of variance of settlement degradation rate across the five variants yields $W = 0.94$ ($p = 0.470$), indicating that the variant groups have statistically indistinguishable within-group variability.

6. Discussion

6.1 Practical Implications for Tramway Asset Management

Three findings of the present analysis translate directly into actionable guidance for tramway asset managers [52]. More broadly, multi-criteria decision-making methods provide a formal basis for converting condition rankings into maintenance decisions, as demonstrated for risk assessment in hazardous-materials transport [53], supplier selection [54], and equipment selection [55]. First, the strong negative correlation between right- and left-rail settlement slopes indicates that single-rail-based maintenance triggers will systematically underestimate the magnitude of the degradation: the twist that develops between the two rails, rather than the absolute settlement of either rail, is the relevant input to vehicle dynamics and to passenger ride-quality models [56]. A direct policy implication is that maintenance thresholds in tramway operating regulations should be reformulated in terms of track twist rather than in terms of per-rail settlement, in line with the EN 13848-1 approach for mainline tracks. Second, the strong age dependence of gauge widening on concrete-slab tracks suggests that gauge-restoring interventions should be scheduled by age rather than by reactive defect counting, and that the concrete-slab variants may benefit from a redesigned rail fastening with a tighter clip pitch. Third, the lifetime-projection layer provides a quantitative basis for prioritization: under the current projection, four high-load, relatively young sections (RF.II-1, RF.III-4, RF.II-2, RF.II-4) should be scheduled for intervention within 10 years, while several older but lower-load ballasted sections can be confidently deferred for more than 2 decades. This prioritization is the condition-side complement to maintenance-scheduling optimization, from integrated production-and-maintenance planning [57] to railway tamping schedules [58, 59].

6.2 Methodological Transferability

The six-layer framework developed in Section 4 is not specific to either the Budapest network or to the particular instrument used. All six layers operate on a single tabular database with columns for section identifier, measurement date, chainage, geometric parameter, and value. Any urban-rail operator running a periodic geometric inspection program – whether with handheld instruments, self-propelled inspection vehicles, or revenue-service axle-box sensors – can construct an equivalent database and apply an equivalent framework. The 25 m segment length, the 0.25 m chainage sampling, and the 3.0 mm intervention threshold are all parameters of the framework that should be re-tuned to local operational conditions. The full statistical pipeline is implemented in Python 3.12 using only open-source libraries (pandas, NumPy, SciPy, statsmodels, matplotlib).

6.3 Limitations of the Framework

Three principal limitations should be acknowledged. First, the 2.3-year campaign window is short relative to the expected 30–40-year service life of the systems under study. While the present analysis provides strong evidence in favor of the linear-degradation model over the exponential within the campaign window, this should not be taken as a refutation of exponential growth on the multi-decade scale; a sub-interval of an exponential curve is well approximated locally by a straight line, and a longer campaign would be required to discriminate between sustained linear growth and a slow acceleration. Second, the unloaded measurement frame cannot capture the track's instantaneous elastic deflection under traffic. In contrast, this elastic component is sub-millimetric under typical light-rail axle loads and is therefore unlikely to alter the conclusions reported here qualitatively. Future work that integrates onboard accelerometer measurements with handheld geometric measurements [48] would constitute a substantial advance. Third, the eighteen-section sample, while spanning a useful range of installation epochs and operational loads, is not large enough to support a fully factorial decomposition of variant, age, and load effects; the partial confounding between ESCRB variant and installation year (the three ESCRB variants entered service in successive technology generations) cannot be fully resolved without an enlarged sample.

6.4 Future Work

Three lines of future work are envisaged. First, the Budapest measurement campaign will continue through 2025 and 2026, materially tightening all bootstrap confidence intervals and, in some cases, enabling meaningful discrimination between the linear and exponential temporal forms. Second, an onboard accelerometer dataset collected on the same sections [48, 60] is matched to the geometric measurements to estimate a quantitative passenger-perception transfer function. Third, a cross-network comparison with at least one other European municipal operator is being initiated, with a view to producing a European-scale ranking of tramway superstructure variants by geometric deterioration rate. Each of these extensions feeds directly into the cognitive-mobility frame: the eventual product is a quantitative coupling between the track's physical state and the cognitive, perceptual, and decision-theoretic outcomes for both passengers and operating personnel.

A related question is how the framework itself should evolve as the monitoring record lengthens. Several of its choices are deliberately conservative, appropriate to a 2.3-year window, and would be revisited once longer series become available. The AIC-based linear-versus-exponential comparison of Layer 6, which at present favors the linear form in the large majority of fits, gains discriminating power as the observation span and the number of epochs grow; with a decade or more of data the same selection step could reliably detect the curvature (acceleration) that a short window cannot resolve, at which point the linear remaining-life extrapolation of Eq. (9) would be replaced by extrapolation of the selected exponential — or a piecewise change-point — model. Longer records would also justify the use of autocorrelation-aware or Bayesian hierarchical trend models in place of the current bootstrap. They would turn the single-threshold remaining-life estimate into a full survival- or hazard-based lifetime distribution with calibrated uncertainty. Finally, a horizon spanning one or more maintenance interventions per section would let the degradation model be re-estimated on each post-intervention segment, so that the framework tracks successive recovery-and-redegradation cycles rather than a single monotone trend. None of these refinements alters the six-layer structure; they are drop-in upgrades of individual layers that the accumulating data will progressively justify.

7. Conclusions

The aim of this work was to provide a firmer statistical basis for prioritizing urban-rail maintenance. The outcome is a six-layer framework that carries the analysis from per-rail descriptive statistics through both-rail unified metrics and an EN 13848-style Track Quality Index, onto bootstrap-validated trend estimation, mixed-effects variance partitioning, and a final lifetime extrapolation against operator-defined intervention thresholds. The complete pipeline was applied to 374,610 geometric measurement points from 18 Budapest tramway sections across 6 superstructure variants.

Part of the contribution is methodological. Both-rail unified metrics – the point-wise absolute mean, the root-mean-square, and the EN 13848 track twist – were defined so that the two rails of a section are read together rather than collapsed into a single average. Because the 200 m segment length prescribed by EN 13848 is usually longer than an entire tramway test section, the Track Quality

Index was recast as the section-mean of the standard deviation over 25 m segments, which keeps the analysis within the EN 13848-1 D1 wavelength band (3–25 m). The benefit is tangible: asymmetries between the two rails that per-rail averaging would otherwise conceal are once again made visible.

The empirical results are best understood in terms of five observations.

Settlement in running rail formations of track is not symmetric. The amount of settlement of the two rails in a track section can differ significantly. In the study presented here, the per-section settlement slopes for the two rails of all 18 track sections were strongly and negatively correlated with each other ($r = -0.864$, $p < 0.0001$, $n = 18$). This means that the sign of the slope of the settlement of one rail is opposite to that for the other rail of the same section of track. As a result, the amount of track twist caused by uneven settlement of the two rails of a track section, EN 13848, will increase with time for all types of track. Hence, it is recommended that any assessment of track subsidence or settlement be carried out on a single rail basis rather than as an average across the two rails.

The results for gauge widening were compared with those for two key measures of deterioration: the worst-case deterioration of either the rails or the sleepers. It was demonstrated that the relationship between superstructure age and the widening of the gauge of BL type of track was the tightest age–parameter relationship within the data set ($R^2 = 0.72$, $p < 0.0001$, $n = 24$). This suggests it would be more appropriate to schedule gauge-restoring work based on the track's age rather than waiting for defects to develop. Fastenings with a tighter clip pitch might also be beneficial.

The mixed-effects models for the development of the track gauge also describe the trend over time and the amount of variance between sections and between years not explained by the trend. The intraclass correlation coefficient (ICC) for the development of the track gauge is high (0.672). This means that after removal of the effect of time and the type of superstructure, two-thirds of the remaining variance is due to the identity of the sections (or the measurements within sections) and the age at which the sections were built. In other words, the development of the two rails of a section (gauge) is not much affected by time. The same does not apply to the development of the two rails of a section with respect to settlement and twist. The random-intercept variance for these two parameters is effectively zero, indicating that the deterioration due to superstructure type and time is already fully captured by the trend.

For all 54 section-metric pairs, a linear and an exponential function was fitted, and the model with the lowest AIC score was chosen. For 94.4% of the section-metric pairs, the linear function had the lowest AIC score (mean $\Delta AIC = +0.56$). Within a single maintenance cycle – here a 2.3-year window – urban-rail geometry degradation can be treated as locally linear, which is precisely the assumption underpinning the lifetime extrapolation used here.

That extrapolation completes the chain. Combining the bootstrap-validated section slopes ($B = 10{,}000$ resamples) with each section's current state, and ranking the projected time to a 3.0 mm unified-settlement threshold, singles out four sections – RF.II-1, RF.III-4, RF.II-2, and RF.II-4 – for intervention within ten years. These share two features: recent installation (2011–2018) and heavy annual loading (4.30–12.84 MGT/year). The ranking gives the operator a defensible, quantitative basis for reordering the maintenance schedule.

None of this is peculiar to Budapest. The same framework can be applied by any operator that performs periodic geometric inspection, and were it adopted more widely, a European-scale ranking of tramway superstructure variants by deterioration rate would come within reach – together with a first step toward a cognitive-mobility-aware predictive-maintenance pipeline that links the physical condition of the track to the quality of the ride as passengers experience it.

Remark: The paper is the continuation of the authors' previous study [61].

List of Symbols

Symbol	Definition / Description
a	Slope of the linear temporal model (mm/year)
$AM_{unified}(s)$	Both-rail unified absolute mean at chainage s (mm)
b	Intercept of the linear temporal model (mm)
B	Number of bootstrap resamples (B = 10,000)
c	Scale parameter of the exponential temporal model (mm)
H	Kruskal–Wallis test statistic
ICC	Intraclass correlation coefficient (dimensionless)
k	Growth-rate parameter of the exponential temporal model (1/year)
$l(s)$	Left-rail settlement (or alignment) value at chainage s (mm)
n	Sample size (number of sections or observations)
p	Significance probability (p-value)
r	Pearson correlation coefficient (right- vs. left-rail settlement slopes)
$r(s)$	Right-rail settlement (or alignment) value at chainage s (mm)
R^2	Coefficient of determination of a regression
$RMS_{unified}(s)$	Both-rail unified root-mean-square at chainage s (mm)
s	Chainage — longitudinal position along the section (m)
a_{us}	Section-level degradation slope of the both-rail unified settlement (mm/year)
t	Time, in years from the section's first measurement (year)
T_{rem}	Projected remaining lifetime of the section (year)
TQI	Track Quality Index of the section (mm)
$TW(s)$	EN 13848 track twist at chainage s (mm)
W	Brown–Forsythe test statistic
x	Value of a geometric parameter at an individual chainage point (mm)
$y(t)$	Value of the summary metric at time t (mm)
y_{cur}	Most recent observed value of the unified settlement (mm)
ΔAIC	Difference in Akaike Information Criterion between two fitted models
ϑ	Intervention threshold for the unified settlement (ϑ = 3.0 mm)
σ	Standard deviation; e.g., $\sigma_{segment}$, the segment standard deviation (mm)
σ^2	Variance; e.g. $\sigma^2_{section}$ and $\sigma^2_{residual}$ (mm^2)
$\langle\cdot\rangle$	Arithmetic mean (averaging operator) over all chainage points of a section
$\mathrm{mean}_{segments}(\cdot)$	Arithmetic mean taken over all valid 25 m segments of the section

List of Abbreviations

Abbreviation	Definition / Description
AIC	Akaike Information Criterion
AM	Absolute mean (as in $AM_{unified}$ – the both-rail unified absolute mean)
ANCOVA	Analysis of covariance
BL	Concrete-slab track sections
CI	Confidence interval
D1	The EN 13848-1 "D1" wavelength band (3-25 m) for track-geometry assessment
EN	European Norm / European Standard (EN 13848, EN 13848-1, EN 13848-5)
ESCRB	Elastically Supported Continuous Rail Bedding (variants I-III)

Abbreviation	Definition / Description
MGT	Million (equivalent) gross tons – annual load, expressed per year
MixedLM	Mixed Linear Model – the implementation name in the *statsmodels* library
OLS	Ordinary Least Squares (regression)
RC	Reinforced concrete (RC sleeper / RC slab)
RF	ESCRB track sections (RF.I, RF.II, RF.III, by ESCRB generation)
RMS	Root-mean-square
SD	Standard deviation (used in "segment-SD")
TW	Track twist (the EN 13848 track-twist parameter)
ZK	Ballasted track sections

Funding
This research received no external funding.

Data Availability Statement
The data supporting the reported results are available from the corresponding author upon reasonable request. The raw geometric measurement data are not publicly available owing to restrictions agreed with the infrastructure operator (BKV Zrt.).

Conflicts of Interest
The authors declare no conflict of interest.

Acknowledgement
The research was supported by the SZE-RAIL Research Team of Széchenyi István University. The authors gratefully acknowledge the operational and technical support provided by BKV Zrt. (the Budapest Transport Company), in particular, by the staff of the Buda Permanent Way Branch, the Pest Permanent Way Branch, and the Track Disturbance Branch.

Declaration on the Use of Artificial Intelligence Tools
During the preparation of this manuscript, the authors used Grammarly and DeepL for language editing and Claude Opus for programming-related auxiliary tasks.

References
[1] Soleimanmeigouni, I., Ahmadi, A., & Kumar, U. (2018). Track geometry degradation and maintenance modelling: A review. *Proceedings of the Institution of Mechanical Engineers, Part F: Journal of Rail and Rapid Transit*, 232(1), 73–102. https://doi.org/10.1177/0954409716657849
[2] Sysyn, M., Przybylowicz, M., Nabochenko, O., & Liu, J. (2021). Mechanism of sleeper-ballast dynamic impact and residual settlements accumulation in zones with unsupported sleepers. *Sustainability*, 13(14), 7740. https://doi.org/10.3390/su13147740
[3] Liao, Y., Han, L., Wang, H., & Zhang, H. (2022). Prediction models for railway track geometry degradation using machine learning methods: A review. *Sensors*, 22(19), 7275. https://doi.org/10.3390/s22197275
[4] Bris-Peñalver, F. J., Verdecia-Peña, R., & Alonso, J. I. (2026). A survey of AI-enabled predictive maintenance for railway infrastructure. *Sensors*, 26(3), 906. https://doi.org/10.3390/s26030906
[5] Ahac, M., & Lakušić, S. (2015). Tram track maintenance-planning by gauge degradation modelling. *Transport*, 30(4), 430–436. https://doi.org/10.3846/16484142.2015.1116464
[6] Kurhan, D., & Kovalskyi, D. (2025). Quasi-static methods for determining the calculated wheel load on the railway track. *Acta Technica Jaurinensis*, 18(1), 38–45. https://doi.org/10.14513/actatechjaur.00769
[7] CEN. (2017). *EN 13848-5:2017. Railway applications – Track – Track geometry quality – Part 5: Geometric quality levels – Plain line, switches and crossings*. European Committee for Standardization.

[8] Esveld, C. (2001). *Modern railway track* (2nd ed.). MRT-Productions.
[9] Fischer, S., & Kocsis Szürke, S. (2023). Detection process of energy loss in electric railway vehicles. *Facta Universitatis, Series: Mechanical Engineering*, 21(1), 81–99. https://doi.org/10.22190/FUME221104046F
[10] Sysyn, M., Gerber, U., Nabochenko, O., & Kovalchuk, V. (2019). Common crossing fault prediction with track-based inertial measurements: statistical vs. mechanical approach. *Pollack Periodica*, 14(2), 15–26. https://doi.org/10.1556/606.2019.14.2.2
[11] Jóvér, V., Major, Z., Németh, A., Kurhan, D., Sysyn, M., & Fischer, S. (2023a). Investigation of "open" superstructure tramway tracks in Budapest. *Infrastructures*, 8(2), 33. https://doi.org/10.3390/infrastructures8020033
[12] Jóvér, V., Major, Z., Németh, A., Kurhan, D., Sysyn, M., & Fischer, S. (2023b). Investigation of the geometrical deterioration of paved superstructure tramway tracks in Budapest (Hungary). *Infrastructures*, 8(8), 126. https://doi.org/10.3390/infrastructures8080126
[13] Jóvér, V., & Fischer, S. (2022). Statistical analysis of track geometry parameters on tramway line no. 1 in Budapest. *The Baltic Journal of Road and Bridge Engineering*, 17(2), 75–106. https://doi.org/10.7250/bjrbe.2022-17.561
[14] Soleimanmeigouni, I., Xiao, X., Ahmadi, A., Xie, M., Nissen, A., & Kumar, U. (2018). Modelling the evolution of ballasted railway track geometry by a two-level piecewise model. *Structure and Infrastructure Engineering*, 14(1), 33–45. https://doi.org/10.1080/15732479.2017.1326946
[15] Jiang, J., Lian, C., Meng, B., Jing, H., Fang, X., & Wang, J. (2025). An approximate solution of the bending of beams on a nonlinear elastic foundation with the Galerkin method. *Journal of Applied and Computational Mechanics*, 11(2), 285–293. https://doi.org/10.22055/jacm.2024.46952.4633
[16] Bai, L., Liu, R., Sun, Q., Wang, F., & Xu, P. (2015). Markov-based model for the prediction of railway track irregularities. *Proceedings of the Institution of Mechanical Engineers, Part F: Journal of Rail and Rapid Transit*, 229(2), 150–159. https://doi.org/10.1177/0954409713503460
[17] Šestáková, J., Ižvolt, L., & Mečár, M. (2019). Degradation – prediction models of the railway track quality. *Civil and Environmental Engineering*, 15(2), 115–124. https://doi.org/10.2478/cee-2019-0015
[18] Ehrhart, U., Knabl, D., & Marschnig, S. (2024). Track deterioration model – state of the art and research potentials. *Infrastructures*, 9(5), 86. https://doi.org/10.3390/infrastructures9050086
[19] Sadeghi, J., & Askarinejad, H. (2011). Development of track condition assessment model based on visual inspection. *Structure and Infrastructure Engineering*, 7(12), 895–905. https://doi.org/10.1080/15732470903194676
[20] Soleimanmeigouni, I., Ahmadi, A., Nissen, A., & Xiao, X. (2020). Prediction of railway track geometry defects: a case study. *Structure and Infrastructure Engineering*, 16(7), 987–1001. https://doi.org/10.1080/15732479.2019.1679193
[21] Šestáková, J., Pultznerová, A., & Mečár, M. (2022). The maintenance of the railway superstructure and its influence on the track geometry of regional line. *Acta Technica Jaurinensis*, 15(3), 162–173. https://doi.org/10.14513/actatechjaur.00664
[22] Marschnig, S., Ehrhart, U., & Offenbacher, S. (2022). Long-term behaviour of padded concrete sleepers on reduced ballast bed thickness. *Infrastructures*, 7(10), 132. https://doi.org/10.3390/infrastructures7100132
[23] Farkas, A. (2020). Measurement of railway track geometry: a state-of-the-art review. *Periodica Polytechnica Transportation Engineering*, 48(1), 76–88. https://doi.org/10.3311/PPtr.14145
[24] Sresakoolchai, J., & Kaewunruen, S. (2022). Railway defect detection based on track geometry using supervised and unsupervised machine learning. *Structural Health Monitoring*, 21(4), 1757–1767. https://doi.org/10.1177/14759217211044492
[25] Wang, Q., Zhao, H., Gong, D., Zhou, J., & Xiao, Z. (2024). Quantitative detection of vertical track irregularities under non-stationary conditions with variable vehicle speed. *Sensors*, 24(12), 3804. https://doi.org/10.3390/s24123804
[26] Berawi, A. R. B., Delgado, R., Calçada, R., & Vale, C. (2010). Evaluating track geometrical quality through different methodologies. *International Journal of Technology*, 1(1), 38–47.
[27] Dawod, A. B. A., & Terdik, G. (2024). Use of zero-crossings segmentation for track quality assessment. *Acta Technica Jaurinensis*, 17(1), 8–21. https://doi.org/10.14513/actatechjaur.00726
[28] Yudariansyah, H., Ismiyati, I., & Narendera, A. (2025). Prediction model for track quality index categories on the northern and southern railway lines of Java. *Periodica Polytechnica Transportation Engineering*, 53(2), 184–193. https://doi.org/10.3311/PPtr.38115
[29] Offenbacher, S., Neuhold, J., Veit, P., & Landgraf, M. (2020). Analyzing major track quality indices and introducing a universally applicable TQI. *Applied Sciences*, 10(23), 8490. https://doi.org/10.3390/app10238490
[30] Sysyn, M., Kovalchuk, V., & Jiang, D. (2019). Performance study of the inertial monitoring method for railway turnouts. *International Journal of Rail Transportation*, 7(2), 103–116. https://doi.org/10.1080/23248378.2018.1514282

[31] Sysyn, M., Nabochenko, O., & Kovalchuk, V. (2020). Experimental investigation of the dynamic behavior of railway track with sleeper voids. *Railway Engineering Science*, 28(3), 290–304. https://doi.org/10.1007/s40534-020-00217-8
[32] Andrade, A. R., & Teixeira, P. F. (2015). Statistical modelling of railway track geometry degradation using hierarchical Bayesian models. *Reliability Engineering & System Safety*, 142, 169–183. https://doi.org/10.1016/j.ress.2015.05.009
[33] Sysyn, M., Nabochenko, O., Kovalchuk, V., Przybyłowicz, M., & Fischer, S. (2021). Investigation of interlocking effect of crushed stone ballast during dynamic loading. *Reports in Mechanical Engineering*, 2(1), 65–76. https://doi.org/10.31181/rme200102065s
[34] Sysyn, M., Nabochenko, O., Kluge, F., Kovalchuk, V., & Pentsak, A. (2019). Common crossing structural health analysis with track-side monitoring. *Communications – Scientific Letters of the University of Žilina*, 21(3), 77–84. https://doi.org/10.26552/com.C.2019.3.77-84
[35] Grohs, G., Pircher, P., Quirchmair, M., Loy, H., Six, K., & Pospischil, F. (2025). Behavior of turnout sleepers in a large-scale ballast box test. *Scientific Reports*, 15, 16717. https://doi.org/10.1038/s41598-025-01751-3
[36] Quezada, J. C., Saussine, G., Breul, P., & Radjaï, F. (2014). Predicting the settlement of coarse granular materials under vertical loading. *Scientific Reports*, 4, 5707. https://doi.org/10.1038/srep05707
[37] Korenjak, A. K., Offenbacher, S., & Marschnig, S. (2024). Detection of short-section ballast breakdown in track: a fractal analysis approach with reduced window size. *Fractal and Fractional*, 8(11), 664. https://doi.org/10.3390/fractalfract8110664
[38] Kou, L., Sysyn, M., & Liu, J. (2024). Influence of crossing wear on rolling contact fatigue damage of frog rail. *Facta Universitatis, Series: Mechanical Engineering*, 22(1), 25–44. https://doi.org/10.22190/FUME220106024K
[39] Wei, Z., Núñez, A., Li, Z., & Dollevoet, R. (2017). Evaluating degradation at railway crossings using axle box acceleration measurements. *Sensors*, 17(10), 2236. https://doi.org/10.3390/s17102236
[40] Liu, X., & Markine, V. L. (2020). Train hunting related fast degradation of a railway crossing – condition monitoring and numerical verification. *Sensors*, 20(8), 2278. https://doi.org/10.3390/s20082278
[41] Zöldy, M. (2024). Changes at mobility space use in the cognitive mobility era. *Acta Technica Jaurinensis*, 17(4), 163–168. https://doi.org/10.14513/actatechjaur.00750
[42] Csete Szalmáné, M. (2024). Exploring the field of cognitive sustainability. *Cognitive Sustainability*, 3(1), 3–9. https://doi.org/10.55343/CogSust.90
[43] Łuczyszyn, K. (2024). Sustainable transport – development and goals. *Cognitive Sustainability*, 3(1). https://doi.org/10.55343/CogSust.92
[44] Zöldy, M., Baranyi, P., & Török, Á. (2024). Trends in cognitive mobility in 2022. *Acta Polytechnica Hungarica*, 21(7), 189–202. https://doi.org/10.12700/APH.21.7.2024.7.11
[45] Macsinka, K. (2025). Mobility impacts of urban development in the agglomeration. *Acta Technica Jaurinensis*, 18(4), 172–179. https://doi.org/10.14513/actatechjaur.00782
[46] Al-lami, A., & Török, Á. (2025). Decomposition of carbon dioxide (CO2) emissions in Hungary: a case study based on the Kaya identity and LMDI model. *Periodica Polytechnica Transportation Engineering*, 53(1), 7–15. https://doi.org/10.3311/PPtr.37552
[47] Taran, I., Olzhabayeva, R., Oliskevych, M., & Danchuk, V. (2023). Structural optimization of multimodal routes for cargo delivery. *Archives of Transport*, 67(3), 49–70. https://doi.org/10.5604/01.3001.0053.7076
[48] Jóvér, V., Kocsis Szürke, S., Hermán, B., Böröcz, P., Kuczmann, M., & Fischer, S. (2025). Vehicle dynamics measurements with a unique measuring system for trams. In M. Zöldy (Ed.), *Proceedings of the 3rd Cognitive Mobility Conference (CogMob 2024)* (Lecture Notes in Networks and Systems, Vol. 1258, pp. 27–41). Springer. https://doi.org/10.1007/978-3-031-81799-1_3
[49] Tánczos, K. (2025). Adapting the ITF's transport policy with a focus on the EU's strategy of sustainable mobility. *Periodica Polytechnica Transportation Engineering*, 53(2), 222–225. https://doi.org/10.3311/PPtr.39780
[50] Metalelektro Méréstechnika Ltd. (2020). *TrackScan ME 4.01 – Operating manual and accuracy specification*. Internal document.
[51] Uranjek, M., & Štrukelj, A. (2025). Evaluation of ballasted railway track response in potentially critical areas using vibration measurements. *Sensors*, 25(14), 4363. https://doi.org/10.3390/s25144363
[52] Božanić, D., Epler, I., Puška, A., Biswas, S., Marinković, D., & Koprivica, S. (2024). Application of the DIBR II–rough MABAC decision-making model for ranking methods and techniques of lean organization systems management in the process of technical maintenance. *Facta Universitatis, Series: Mechanical Engineering*, 22(1), 101–123. https://doi.org/10.22190/FUME230614026B
[53] Vahabzadeh, S., Sami Haghshenas, S., Javadi Ghoushchi, S., Guido, G., Simic, V., & Marinković, D. (2025). A new framework for risk assessment of road transportation of hazardous substances. *Facta Universitatis, Series: Mechanical Engineering*, 23(3), 479–509. https://doi.org/10.22190/FUME240801007V

[54] Bošković, S., Jovčić, S., Simić, V., Švadlenka, L., Dobrodolac, M., & Bacanin, N. (2025). A new criteria importance assessment (CIMAS) method in multi-criteria group decision-making: criteria evaluation for supplier selection. *Facta Universitatis, Series: Mechanical Engineering*, 23(2), 335–349. https://doi.org/10.22190/FUME230730050B

[55] Chakraborty, S., & Saha, A. K. (2024). Selection of forklift unit for transport handling using integrated MCDM under neutrosophic environment. *Facta Universitatis, Series: Mechanical Engineering*, 22(2), 235–256. https://doi.org/10.22190/FUME220620039C

[56] Bian, J., Gu, Y., & Murray, M. H. (2013). A dynamic wheel-rail impact analysis of railway track under wheel flat by finite element analysis. *Vehicle System Dynamics*, 51(6), 784–797. https://doi.org/10.1080/00423114.2013.774031

[57] Babaeimorad, S., Fattahi, P., Fazlollahtabar, H., & Shafiee, M. (2024). An integrated optimization of production and preventive maintenance scheduling in Industry 4.0. *Facta Universitatis, Series: Mechanical Engineering*, 22(4), 711–720. https://doi.org/10.22190/FUME230927014B

[58] Khosravi, M., Ahmadi, A., Kasraei, A., & Nissen, A. (2024). Optimisation of railway tamping scheduling. *Heliyon*, 10(23), e40844. https://doi.org/10.1016/j.heliyon.2024.e40844

[59] Famurewa, S. M., Xin, T., Rantatalo, M., & Kumar, U. (2015). Optimisation of maintenance track possession time: a tamping case study. *Proceedings of the Institution of Mechanical Engineers, Part F: Journal of Rail and Rapid Transit*, 229(1), 12–22. https://doi.org/10.1177/0954409713495667

[60] Kliuiev, S., Semenov, S., Mikhailov, E., Dižo, J., Blatnický, M., & Ishchuk, V. (2024). Increasing the traffic safety level of rolling stock by wheel condition monitoring using an automated measuring complex. *Communications – Scientific Letters of the University of Žilina*, 26(3), B167–B174. https://doi.org/10.26552/com.C.2024.031

[61] Révész-Jóvér, V., & Fischer, S. (2026). Asymmetric Track Geometry Degradation of Tramway Superstructure Systems: A Statistical Reassessment from Repeated Handheld Measurements in Budapest. *5th Cognitive Mobility Conference (CogMob 2026)*, submitted manuscript under review.